Competing spatial and temporal instabilities in a globally coupled bistable semiconductor system near a codimension-two bifurcation

S. Bose,[1] P. Rodin,[2] and E. Schöll[1]
[1]*Institut für Theoretische Physik, Technische Universität Berlin, Hardenbergstrasse 36, D-10623, Berlin, Germany*
[2]*Ioffe Physicotechnical Institute, Politechnicheskaya 26, St. Petersburg 194021, Russia*
(Received 27 March 2000)

We study complex spatiotemporal dynamics in a globally coupled bistable reaction-diffusion model on a two-dimensional spatial domain. It is demonstrated that complex behavior appears near a codimension-two bifurcation point due to the competition of spatial and temporal instabilities. We derive sufficient conditions for the appearance of mixed spatiotemporal modes, and clarify the origin of a menagery of complex dynamics, such as periodic and chaotic oscillations of current filaments, low-dimensional spatiotemporal chaos including a Shil'nikov attractor, and periodic back-and-forth motion of current density fronts. Such dynamics is found in a wide range of domain sizes for square and rectangular domains. The type of dynamics is sensitive to small variations in the domain shape. We discuss and explain the differences between spatiotemporal dynamics on one-dimensional and two-dimensional domains.

PACS number(s): 05.70.Ln, 72.20.Ht, 85.30.−z

I. INTRODUCTION

Spatially extended nonlinear dynamic systems may exhibit a variety of different instabilities. Complex spatiotemporal behavior is expected if an instability breaking the spatial symmetry interacts with a temporal instability breaking the time translation symmetry [1–16]. This is the case near the codimension-two (CT) bifurcation where those two instabilities coincide. Recently the dynamics in the vicinity of such bifurcation points of higher codimension has been investigated theoretically [13–16] as well as experimentally for various physical [9–11] and chemical systems [6–8]. A widely studied system is given by the following two-component activator-inhibitor system with local diffusive coupling [1,2,15,16]

$$\tau_a \frac{\partial a}{\partial t} = l_a^2 \Delta a + f(a,u), \tag{1}$$

$$\tau_u \frac{\partial u}{\partial t} = l_u^2 \Delta u + g(a,u), \tag{2}$$

where a and u are the activator and the inhibitor, respectively, and τ_a, τ_u and l_a, l_u determine the respective relaxation times and diffusion lengths. This system exhibits a codimension-two Turing-Hopf bifurcation [2] where the conditions of a spatial Turing instability [17] with a certain wavelength $l_T \sim \sqrt{l_a l_u}$ and a temporal Hopf bifurcation with a certain frequency $\omega \sim 1/\sqrt{\tau_a \tau_u}$ are met simultaneously. An amplitude equation analysis [2,12,15] predicts the appearance of mixed Turing-Hopf modes which represent periodic or chaotic oscillations of localized Turing patterns. Periodic mixed Turing-Hopf modes and chaotic transients preceding the periodic asymptotic motion have also been found by direct numerical simulations on a one-dimensional (1D) spatial domain [16].

For a globally coupled system the Turing instability is suppressed, and little is known about the conditions under which mixed spatio-temporal modes should be found. The purpose of the present paper is to investigate those conditions in a bistable system with a global mechanism of inhibition given by an integral constraint imposed on the internal dynamics:

$$\tau_u \frac{du}{dt} = \frac{1}{A} \int_G dx dy \, g(a(x,y,t),u(t)), \tag{3}$$

where $\int_G dx dy$ denotes integration over a spatial domain G of area A. Equation (3) replaces the local inhibitor Eq. (2).

In the model (1),(3) the inhibitor $u(t)$ is a global variable depending upon the spatially averaged activator $a(x,y,t)$. The Hopf bifurcation of the uniform state remains as in the locally inhibited model (1), (2), but instead of a spatial Turing instability at finite wavelength $l_T \sim \sqrt{l_a l_u}$ the system (1),(3) experiences a long-wavelength instability which may be regarded as limit case of a Turing instability for $l_u \to \infty$. The wavelength of the spatial instability l_G is therefore determined by the system dimension L, where $l_G = 2L$ and $l_G = L$ for Neumann and Dirichlet boundary conditions, respectively. The length scale of the asymptotic stationary pattern evolving from the initial instability is determined by the global constraint (3).

Global coupling has been widely recognized as an important factor of spatiotemporal dynamics in extended systems and studied for different models [18–33]. Equations (1),(3) represent a basic model of a globally coupled bistable medium which is relevant for current density dynamics in large-area bistable semiconductor systems [29–33] and electrochemical systems [27], where global coupling is due to the external electric circuit, as well as chemical reaction systems, where global coupling may be light induced [25] or imposed via the gas phase [22]. In this article we focus on the case of bistable semiconductors. Then Eq. (1) determines the dynamics of an internal, spatially distributed variable $a(x,y,t)$, where x,y are the coordinates in the plane perpendicular to the direction of current flow z (Fig. 1). The physical meaning

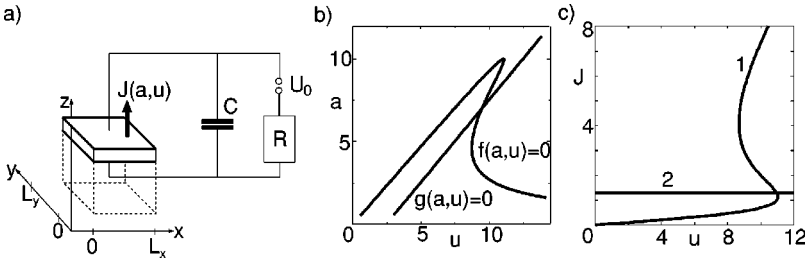

FIG. 1. (a) Sketch of a bistable semiconductor operated in an external circuit with capacitance C, load resistance R and bias U_0. (b),(c) Null isoclines of the model Eqs. (6),(7) in the (a,u) plane and the corresponding (J,u) representation in terms of the local current-voltage characteristic $J(u)$ (curve 1) and the load line (curve 2), respectively. Parameters: $T=0.05$, $J_0=1.25$.

of the variable a might be electron temperature [34] or concentration of excess carriers [35] in bulk semiconductors, charge density stored in the quantum well of double-barrier resonant tunneling structures [36,37,33], interface charge density in the heterostructure hot electron diode [38], or the voltage across one of the pn junctions in thyristors [39,30,32], etc. The variable $a(x,y)$ together with the voltage drop u across the device determines the current density $J(a,u)$ at a given point (x,y). The respective uniform stationary current-voltage characteristic $J(u)=J[a(u),u]$ can be found using the condition $f(a,u)=0$ to express $a(u)$. It may result in either S-shaped or Z-shaped bistable characteristics $J(u)$ [33]. The global coupling is due to the external circuit in which the semiconductor system is operated, and Eq. (3) takes the form of Kirchhoff's law:

$$\tau_u \frac{du}{dt} = U_0 - u - RA\langle J(a;u)\rangle, \quad \tau_u \equiv RC,$$

$$\langle J\rangle \equiv \frac{1}{A}\int_G dxdy J(a,u), \tag{4}$$

where R is the series load resistance, C is the capacitance of the external circuit, U_0 is the applied voltage, and G is a 2D spatial domain in the plane perpendicular to the direction of the current flow [see Fig. 1(a)]. The model (1),(4), originally suggested for semiconductors with overheating instabilities [34], has been later advanced for a wide class of semiconductor systems exhibiting both S- and Z-shaped bistability (see Refs. [29,33,40], and references therein). In this paper we focus on S-shaped bistability. The model (1),(4) can describe a menagery of spatial and temporal patterns in semiconductors such as current filaments, transverse current density fronts, and spatially uniform current oscillations [41]. A mixed spatiotemporal mode corresponding to large-amplitude relaxation-type oscillations of a current filament (spatiotemporal spiking) has also been found in this model for 1D spatial domains [38,42].

The linear stability of stationary current filaments on 2D domains has been studied analytically and numerically [29] in the framework of the globally coupled model (1),(4). Here we investigate the nonlinear dynamical behavior of 2D current density patterns, in particular in the vicinity of the CT bifurcation point. We derive criteria for the onset of mixed spatiotemporal modes and illustrate our findings by numerical simulations of the model on 2D domains. We show that competition between spatial and temporal instabilities gives rise to complex spatiotemporal behavior of transverse current density patterns such as periodic oscillations of current filaments, back-and-forth motion of current density fronts, as well as various regimes of spatiotemporal chaos.

In the following we assume current-controlled conditions $(R\to\infty,\ U_0\to\infty,\ U_0/R\to J_0)$, since these are known to provide the most efficient global coupling [29], and use the model functions

$$f(a,u) = \frac{u-a}{(u-a)^2+1} - Ta, \quad J(a,u) = u-a, \tag{5}$$

originally derived for the heterostructure hot electron diode [38]. A nonpolynomial local kinetic function as, e.g., in Eq. (5) is typical for nonlinear charge transport in various semiconductor systems [34,39,43]. In dimensionless form, our model equations (1),(4) thus take the form

$$\frac{\partial a}{\partial t} = \Delta a + \frac{u-a}{(u-a)^2+1} - Ta, \tag{6}$$

$$\frac{du}{dt} = \alpha(J_0 - u + \langle a\rangle), \quad \alpha \equiv A/C. \tag{7}$$

Figures 1(b) and 1(c) depict the null isoclines of the system (6),(7) in the (a,u) plane, and the equivalent representation in the (J,u) plane in terms of the S-shaped current-voltage characteristic $J=J(u)$ and the load-line, respectively. The latter representation is physically more intuitive and will be used in the following. We consider rectangular spatial domains with transverse dimensions L_x, L_y and assume Neumann boundary conditions. The dynamics is determined by two model parameters α, J_0, i.e., the inverse relaxation time of the inhibitor u and the imposed current controlling the general excitation level, respectively, and the domain size L_x, L_y. The parameter T controls the bistability range; $T=0.05$ is used throughout the paper.

The paper is organized as follows. In Sec. II we consider the fixed points of the model (6),(7), i.e., uniform steady states and stationary current filaments. We discuss spatial and temporal instabilities of those states and derive an analytic criterion for the onset of complex spatiotemporal dynamics. In Sec. III we consider fully developed nonlinear spatiotemporal dynamics on square domains $(L_x=L_y)$ and analyze bifurcation scenarios leading to different regimes of intermittent and chaotic behavior. In Sec. IV we focus on spatiotemporal dynamics in rectangular systems $(L_x>L_y)$ and, in the limit case of $L_x \gg L_y$, study dynamics on 1D domains. Hereby we elaborate and clarify the differences in spatiotemporal dynamics on 1D and 2D domains. In Sec. V we summarize our results and briefly survey alternative mechanisms of complex current density dynamics in bistable semiconductors.

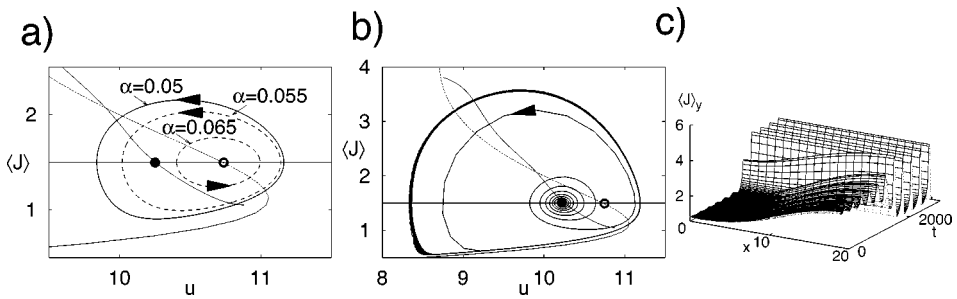

FIG. 2. (a) Phase portraits of uniform oscillations for $J_0=1.5$, $L_x=L_y=20$, and different values of α. In the $(\langle J\rangle,u)$ plane spatially stable and unstable limit cycle oscillations are shown by solid and long dashed lines, respectively, they become stable at $\alpha\approx 0.05$. The uniform fixed point (empty circle) is temporally and spatially unstable for the parameters chosen (critical value $\alpha_u\approx 0.068$). The nonuniform fixed point corresponding to a stationary filament (full circle) loses stability at $\alpha\approx 0.0259$. The uniform and the nonuniform fixed points are given by the intersections of the load line $\langle J\rangle=J_0$ with the uniform (unstable parts: thin dotted line, stable parts: thin solid line) and the filamentary (thin solid line) current-voltage characteristics, respectively. (b) Phase portrait for $J_0=1.5$, $L_x=L_y=20$, $\alpha=0.023$. The trajectory spiralling out of the nonuniform fixed point depicts an oscillatory instability of the stationary filament evolving into a uniform limit cycle. (c) Spatiotemporal plot of the trajectory depicted in (b). The current density $\langle J(x,y,t)\rangle_y$ averaged over the y coordinate is shown.

II. FIXED POINTS AND THEIR BIFURCATIONS

A. Uniform steady state

In this section we consider spatially uniform and nonuniform fixed points of our system and analyze their possible bifurcations. The uniform steady state (a_0,u_0) is given by $f(a_0,u_0)=0$, $J(a_0,u_0)=J_0$ and corresponds to the intersection of the load line with the uniform current-voltage characteristic [Fig. 1(b)]. A linear stability analysis of Eqs. (6),(7) shows (e.g., Ref. [41]) that this state is unstable with respect to spatially inhomogeneous fluctuations leading to a stationary current filament if

$$\left(\frac{\pi}{L}\right)^2<\partial_a f,\quad \partial_a f|_{(a_0,u_0)}\equiv\frac{J_0^2-1}{(1+J_0^2)^2}-T,$$

$$L\equiv\max[L_x,L_y]. \tag{8}$$

The condition $\partial_a f>0$ is met for the middle branch of the current-voltage characteristic [29] which is consequently unstable for sufficiently large L. The minimum system size $L=L_{cr}(J_0)=\pi/\sqrt{\partial_a f}$ which allows for a transverse instability depends on J_0. A transverse instability is never possible for $L<L_{\min}=11.5$ for the value of $T=0.05$ chosen. Thus $L_{\min}$ has the meaning of a critical transverse diffusion length and represents a natural scale for the size L_x, L_y of the spatial domain.

The uniform steady state (a_0,u_0) may also experience a Hopf bifurcation leading to uniform limit-cycle oscillations if the relaxation time of the inhibitor α^{-1} is sufficiently slow [41], i.e., for

$$\alpha<\partial_a f. \tag{9}$$

We denote the critical value by $\alpha_u(J_0)\equiv\partial_a f$. The oscillation amplitude increases with decreasing α [Fig. 2(a)], and eventually typical nonlinear relaxation oscillations are established. These uniform limit-cycle oscillations can be unstable with respect to transverse spatial perturbations. Let us linearize Eqs. (6),(7) in the vicinity of the limit cycle solution $\tilde{a}(t)$, $\tilde{u}(t)$, assuming $a(x,t)=\tilde{a}(t)+\delta a(t)\cos(\pi nx/L)$, $u(t)=\tilde{u}(t)+\delta u(t)$, where $\delta a(t),\delta u(t)$ are the amplitudes of perturbations with wave vector $k=\pi n/L$, where n is an integer. This yields

$$\frac{d}{dt}\delta a(t)=\left[\widetilde{\partial_a f}(t)-\left(\frac{\pi n}{L}\right)^2\right]\delta a+\widetilde{\partial_u f}(t)\,\delta u,$$

$$\widetilde{\partial_{a,u} f}(t)\equiv\partial_{a,u} f(\tilde{a}(t),\tilde{u}(t)), \tag{10}$$

$$\frac{d}{dt}\delta u(t)=-\alpha\,\delta u. \tag{11}$$

Here $\widetilde{\partial_a f}(t)$ and $\widetilde{\partial_u f}(t)$ are periodic functions in time. Since the relaxation dynamics of δu is uncoupled from δa, a sufficient condition for spatial instability of the limit cycle can be written as

$$\left(\frac{\pi}{L}\right)^2<\widetilde{\partial_a f}(t). \tag{12}$$

Note that Eq. (12) resembles Eq. (8). If condition (12) is satisfied for the uniform fixed point (a_0,u_0), it is also satisfied for uniform limit cycles of sufficiently small amplitude which have bifurcated from this fixed point. Therefore small-amplitude limit cycles near the bifurcation threshold are always spatially unstable. For limit cycles of arbitrary amplitude the sign of $\widetilde{\partial_a f}-(\pi/L)^2$ is not fixed and one should apply a Floquet analysis, or simply integrate Eq. (10) over one period to evaluate stability. For the limit case of large-amplitude relaxation oscillations with $\alpha\ll\partial_a f$ the spatial stability can be demonstrated by the following Heuristic argument. For such oscillations one cycle in phase space consists of slow stages corresponding to relaxation of u along the stable branches of the uniform current-voltage characteristic $a=a_{\rm on}(u)$ and $a=a_{\rm off}(u)$, and fast stages corresponding to fast relaxation of a at $u=$const. Since $\partial_a f<0$ for $a=a_{\rm on,off}$ and the contribution of fast stages can be neglected when integrating Eq. (10) over one period, we see that the perturbation δa decreases. The transition from spatially unstable to spatially stable limit cycles with increasing amplitude is illustrated in Fig. 2(a). Figures 2(b), 2(c) visualizes the tran-

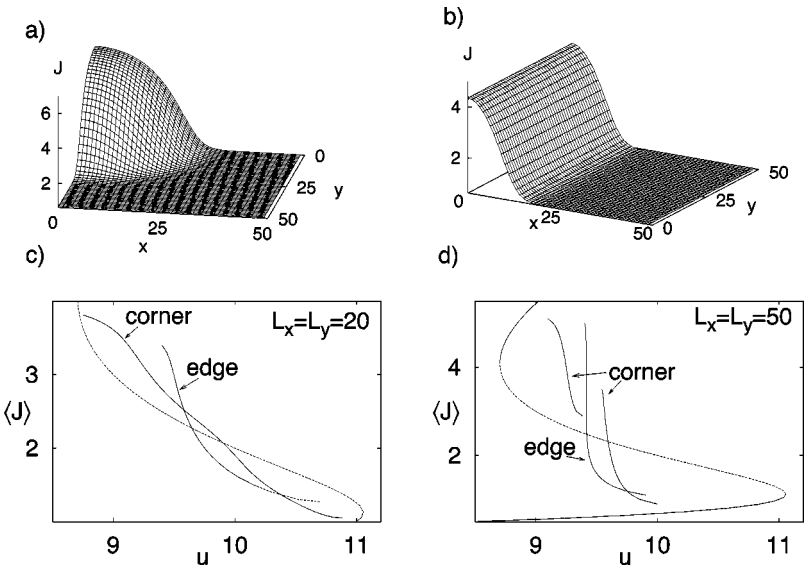

FIG. 3. Stationary corner filament (a) and edge current layer (b), and the associated current-voltage characteristics for $L_x=L_y=20$ (c) and $L_x=L_y=50$ (d). Branches corresponding to transversally unstable edge current layers are marked by dotted lines. The uniform S-shaped current-voltage characteristic is also shown.

sient leading from a temporally unstable stationary filament to a stable uniform limit cycle.

B. Stationary current filaments

The stationary current filament bifurcating from the uniform steady state according to Eq. (8) may be stable or unstable. A necessary condition for stability of a filament on a convex 2D domain in the regime of strong global coupling ($R\to\infty$) is that the differential conductance of the filament $\sigma_d \equiv A(d\langle J\rangle/du)$ is negative and the extrema of the current density distribution are located at the boundary of the domain [29]. Multifilamentary states (with several extrema) are unstable according to the winner-takes-all principle [20]; filaments with an extremum inside the domain are unstable with respect to translation and are eventually attracted by the boundaries [29]. On a rectangular domain stationary current density configurations are either corner filaments [Fig. 3(a)] or edge current layers [Fig. 3(b)]. The respective current-voltage characteristics are shown in Figs. 3(c),3(d) for two different systems sizes $L_x=L_y=20$ and $L_x=L_y=50$. The corner filament is stable in the whole interval of currents. With increasing system size the continuous branch of the current-voltage characteristic [Fig. 3(c)] splits into two separate branches corresponding to a hot (high current density) corner filament and a cold (low current density) corner filament [Fig. 3(d)]. The edge current layer is unstable with respect to spatial perturbations which break the uniformity of the current density distribution along the y axis, transforming the edge current layer into a corner filament if its differential conductance σ_d is sufficiently low. Unstable parts of the current-voltage characteristic are shown in Figs. 3(c),3(d) by dotted lines. On rectangular domains ($L_x>L_y$) one should distinguish between edge current layers parallel to the long and short edge, respectively. Generally, the latter ones are more stable. For $L_y<L_{\min}$ only edge current layers parallel to the short edge are possible and, generally, any type of current density distribution becomes uniform along the y axis which renders spatiotemporal dynamics effectively one dimensional. The type of bifurcation leading to a stationary current filament depends on the system dimensions. For L_x, L_y close to $L_{\min}$ this bifurcation is supercritical as a function of the control parameter J_0, and the stationary patterns have small modulation amplitudes. With increasing L the bifurcation becomes subcritical, resulting in large-amplitude patterns (e.g., see Refs. [44,45]). Sweeping the current J_0 up and down then leads to hysteresis [see Figs. 3(c),3(d)]. It is important to note that large-amplitude patterns arising via subcritical bifurcations cannot be appropriately described by analytical techniques based on expansions near the uniform reference state (a_0,u_0), such as the amplitude equation formalism.

The linearized dynamics near the nonuniform stationary patterns will be shown to have a crucial impact on the possibility of complex spatiotemporal behavior, and we shall now discuss it in some detail. Both corner filaments and edge current layers are unstable in the voltage-controlled regime. This instability is due to a single unstable eigenmode $\Psi_1(x,y)$ with eigenvalue $\lambda_1>0$ [29], corresponding to the ''ground state.'' Hence $\Psi_1(x,y)\geqslant 0$ and it is associated with expansion or shrinking of the current filament. The second eigenmode $\Psi_2(x,y)$ has a negative eigenvalue $\lambda_2<0$. $\Psi_2(x,y)$ changes sign in the interior ot the domain (e.g., on a 1D domain it has one node) and corresponds to softening or sharpening of the current density profile near the filament border. Since $\Psi_2(x,y)$ is not of fixed sign, it cannot be effectively suppressed by an integral constant. In particular, this mode describes the very last stage of current filament growth from the uniform state. In the presence of global coupling the eigenvalues generally become complex. The modes Ψ_i are then mixed by coupling, but they still provide intuitive insight into the linearized dynamics of the globally coupled system [29]. In the regime of strong global coupling (as for $R\to\infty$) the first mode $\Psi_1(x,y)$ is suppressed by the global constraint imposing conservation of the total current, but for sufficiently small α an oscillatory instability due to the delay in the inhibition is possible. If only the lowest, unstable eigenmode $\Psi_1(x,y)$ is taken into account, the general criterion for the oscillatory instability of a current filament described by Eqs. (1),(4) is given by [29]

$$-\sigma_u + C\lambda_1/\tau_a > R^{-1}, \quad \sigma_u \equiv A\langle \partial_u J(a,u)\rangle. \qquad (13)$$

For our model (6),(7) this criterion takes the simple form

$$\alpha < \lambda_1 . \tag{14}$$

We denote the critical values by $\lambda_1 \equiv \alpha_f^c(J_0,L)$ and $\alpha_f^e(J_0,L)$ for corner filaments and edge current layers, respectively. In the one-mode approximation the eigenvalue λ_1 is connected to the differential conductance of a filament σ_d by the approximate expression

$$\sigma_d \approx \sigma_u - A\frac{\langle \partial_u f \cdot \Psi_1 \rangle \langle \partial_a J \cdot \Psi_1 \rangle}{\lambda_1}. \tag{15}$$

[Note that Eqs. (14), (15) are also applicable to the uniform state on the middle branch of the current-voltage characteristic; in this case $\Psi_1 \equiv 1$, $\lambda_1 \equiv \partial_a f$.] For a sufficiently large system, on the middle part of the filamentary branch σ_d is negative and of large absolute value, and therefore λ_1 is small. The physical reason for this is as follows: the current filament has a sharp profile with a narrow transition layer connecting flat on- and off-states. In an infinite system such a profile would be of neutral stability ($\lambda_1 = 0$) due to translation invariance. In a finite system λ_1 becomes positive due to the interaction with the boundaries, but remains small. As a result, an oscillatory instability of such a nonuniform steady state occurs for $\alpha_f = \lambda_1$, which is smaller than the critical value $\alpha_u = \partial_u f$ leading to an oscillatory instability of the uniform state. Thus for $\alpha_f < \alpha < \alpha_u$ there is bistability between a stationary filament and uniform relaxation oscillations. With decreasing α the stationary filament experiences an oscillatory instability, but in general the current density oscillations eventually become uniform, and no complex spatiotemporal behavior arises [29,30,33]. This scenario should be regarded as typical for the oscillatory instability of a stationary filament [Figs. 2(b),2(c)].

However, this conclusion holds only for wide filamentary patterns with sharp boundaries and is not applicable to narrow filaments whose differential conductance σ_d might be comparable to that of the uniform unstable branch of the current-voltage characteristic [see Figs. 3(c),3(d)]. For such narrow filaments both situations $\alpha_f < \alpha_u$ and $\alpha_u < \alpha_f$ are possible. Also, a stationary filament might be stable with respect to small perturbations ($\alpha > \alpha_f$) but unstable with respect to sufficiently large ones. In this case its basin of attraction is bounded by an unstable periodic orbit which corresponds to a breathing filament. This case has been discussed in detail in Ref. [42] for 1D domains.

C. Codimension-two point in the parameter space

The conditions for spatial (8) and temporal (9) instabilities of the uniform fixed point may coincide in a codimension-two (CT) bifurcation point denoted by a superscript star:

$$\alpha^\star = \alpha_u(J_0^\star) = \left(\frac{\pi}{L}\right)^2. \tag{16}$$

For given $L = \max(L_x, L_y) = L_{cr}$ this happens for two values $J_0^\star$ which are defined by Eq. (8) and located near the turning points of the current-voltage characteristic at $J_0 = 1.12$ and $J_0 = 4.09$, respectively [see Fig. 4(a)]. Periodic or chaotic

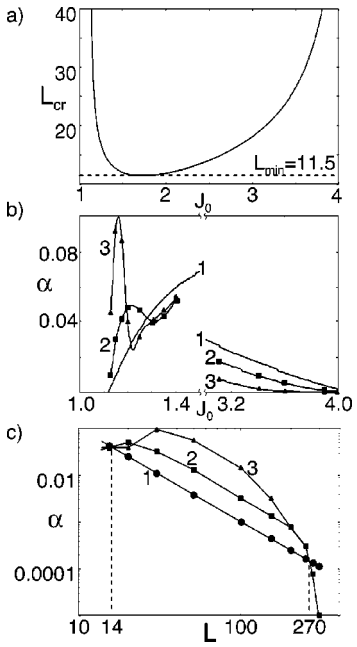

FIG. 4. (a) Minimum system size $L_{cr} = \pi(\partial_a f)^{-1/2}$ allowing for a spatial instability of the uniform steady state as a function of J_0. (b) Thresholds for oscillatory instabilities of the uniform fixed point [$\alpha_u(J_0)$, curve 1], corner filaments ($\alpha_f^c[J_0, L_{cr}(J_0)]$, curve 2) and edge current layers ($\alpha_f^e[J_0, L_{cr}(J_0)]$, curve 3) as a function of the current density J_0 for 2D square domains. The threshold values of α are shown at both codimension-two points. (c) Thresholds for oscillatory instabilities of the uniform fixed point ($\alpha_u[J_0^\star(L)]$, curve 1), corner filaments [$\alpha_f^c[J_0^\star(L), L]$, curve 2] and edge current layers ($\alpha_f^e[J_0^\star(L), L]$, curve 3) as a function of the system size $L = L_x = L_y$ at the lower codimension-two point (double-logarithmic plot).

mixed spatiotemporal modes appear near the CT point if the following condition is met:

$$\alpha_u^\star < \alpha_f^{c,e}(J_0^\star, L) \tag{17}$$

for both corner filament and edge current layers. Indeed, if the criterion (17) is satisfied there is a parameter window $\alpha_u^\star < \alpha < \alpha_f^{c,e}(J_0^\star, L)$ where the uniform state is spatially unstable (but temporally stable with respect to uniform fluctuations) and the stationary filament is temporally unstable, thus the system has no fixed point attractors.

The dependencies $\alpha_f^{c,e}[J_0, L_{cr}(J_0)]$ have been calculated numerically at the CT point for corner and edge filaments on square domain and are shown together with $\alpha_u(J_0)$ in Fig. 4(b). The criterion (17) is met only near the left one of the two CT points, which corresponds to the lower value of current $J_0^\star$. In Fig. 4(c) the critical values $\alpha_f^{c,e}[J_0^\star(L), L]$, $\alpha_u[J_0^\star(L)]$ calculated at the CT point are presented as functions of L. The criterion (17) is satisfied in the interval $14 < L < 270$. This implies that complex spatiotemporal behavior occurs neither for small-amplitude patterns at $L \sim L_{\min}$ nor in large systems $L \gg L_{\min}$. Generally, $\alpha_f / \alpha_u \to 0$ for $L \to \infty$ since the asymptotic behavior of $\alpha_f \sim \exp(-L/L_{\min})$ is exponential [29] but $\alpha_u[J_0^\star(L)]$ decays algebraically as L^{-2}.

The criterion (17) can be also reformulated without direct reference to the CT point. For given J_0 and L_x, L_y complex spatiotemporal behavior occurs if

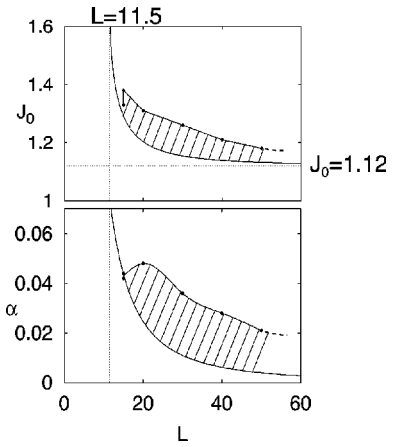

FIG. 5. Regime of complex spatiotemporal dynamics (hatched) in two projections of the (J_0,α,L) parameter space for square domains $L=L_x=L_y$. The curve of codimension-two points, Eq. (16), is shown as the solid line without circles.

$$\alpha_u(J_0)<\alpha<\alpha_f^{e,c}(J_0,L) \quad \text{and} \quad L>L_{cr}(J_0). \tag{18}$$

In the opposite case $\alpha_f^{e,c}<\alpha<\alpha_u$ we expect bistability between a stationary filament and uniform oscillations but no mixed modes.

The criteria (17), (18) represent *sufficient* but not *necessary* conditions for the onset of complex spatiotemporal dynamics. Generally, complex dynamics can also occur for $\alpha_f<\alpha_u$ if the stationary filament is stable only with respect to *small* fluctuations but unstable with respect to large ones (which implies an unstable periodic orbit forming the boundary of its basin of attraction). Complex dynamics can also result from the spatial instability of uniform limit-cycle oscillations but not of the uniform fixed point and can thus occur for $\alpha<\alpha_u<\alpha_f$. Special attention should be given to the situation when Eq. (17) is satisfied only for one type of stationary patterns. Despite these restrictions, the criteria (17), (18) are important for understanding the origin of complex spatiotemporal dynamics. In the following sections we will compare our theoretical predictions based on these criteria with numerical simulations, and will show that the criterion (17) always applies.

III. COMPLEX SPATIOTEMPORAL DYNAMICS ON SQUARE DOMAINS

A. Survey of different regimes in the parameter space

In this section we survey spatiotemporal dynamics on square domains $L_x=L_y=L$. Equations (6),(7) have been solved numerically using slight perturbations of the unstable uniform state (a_0,u_0) as initial condition. The regime in the parameter space (J_0,α,L) where complex current density dynamics—both periodic and chaotic—is found is hatched in Fig. 5. This regime is located in the vicinity of the curve of codimension-two points (16) where spatial (8) and temporal (9) instabilities of the uniform fixed point coincide. In accordance with our theoretical prediction, complex spatiotemporal behavior occurs only near the CT points corresponding to the lower value of $J_0^\star$, where the condition (17) is met, i.e., near the right turning point of the S-shaped current-voltage characteristic [Fig. 1(c)].

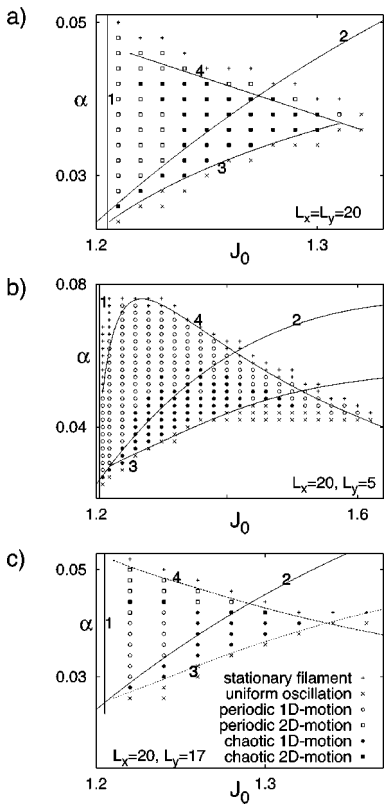

FIG. 6. Regimes of complex spatiotemporal dynamics in the (α,J_0) plane. The boundaries of spatial instability of the uniform steady state (a_0,u_0) (curve 1), Hopf bifurcation of the uniform steady state (curve 2), spatial instability of uniform limit-cycle oscillations (curve 3), and oscillatory instability of stationary current filaments (curve 4) are indicated. (a) 2D square domain $L_x=L_y=20$ (corner filaments). (b) quasi-1D domain $L_x=20$, $L_y=5$ (edge current layers). (c) Rectangular domain with $L_x=20$, $L_y=15$; the spatiotemporal dynamics is effectively 1D (edge current layer mode) for small α and 2D (corner filament mode) for large α.

Complex spatiotemporal dynamics on square domains is always associated with a corner filament: the current density distribution is symmetrical along the diagonal of the domain and the maximum is located in one of the corners. The dynamics generally includes two coupled modes: a nonuniform mode associated with a stationary (not necessarily stable) filament and a uniform mode associated with damped or limit-cycle oscillations. This indicates the low dimensional character of spatiotemporal dynamics.

Figure 6 gives a more detailed account of the different regimes of dynamic behavior. Figure 6(a) specifies points in the (α,J_0) parameter space where stationary filaments, uniform limit cycle oscillations, and periodic or chaotic spatiotemporal dynamics are found for $L_x=L_y=20$. The boundaries of the spatial (curve 1) and temporal (curve 2) instability of the uniform fixed point, of the spatial instability of uniform oscillations (curve 3) and of the temporal instability of stationary corner filaments (curve 4) are also shown. The location of these boundaries clearly indicates that complex spatiotemporal dynamics occurs due to the spatial instability of the uniform fixed point at the left boundary, and via instability of the uniform limit-cycle oscillations at the lower boundary. The corresponding boundaries of stability (curves 1 and 3, respectively) strictly coincide with the respective

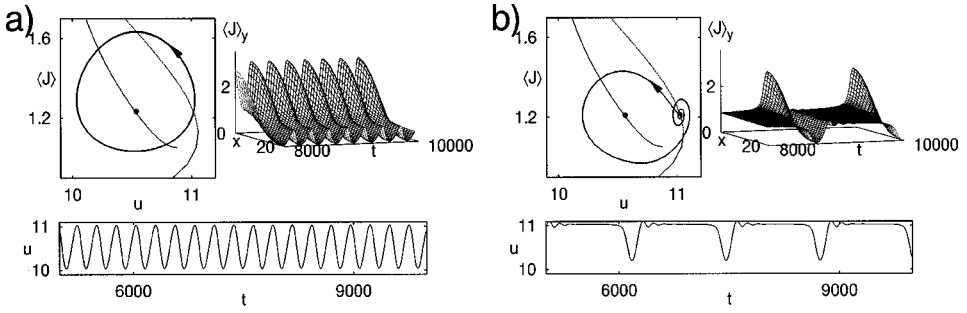

FIG. 7. Spatiotemporal dynamics visualized by phase portraits $(\langle J\rangle,u)$, spatiotemporal plots of the current density $\langle J(x,y,t)\rangle_y$ averaged over the y coordinate, and time series of the voltage $u(t)$. (a) Periodic breathing, (b) periodic spiking of a corner current filament on a 2D square domain ($L_x=L_y=20$, $\alpha=0.04$). Parameters (a) $J_0=1.29$, (b) $J_0=1.21$.

boundaries of the numerically found regime of complex dynamics for all L. At the upper boundary the transients of complex behavior are associated with the oscillatory instability of a stationary filament. However, the respective curve 4 does not exactly coincide with the boundary of complex dynamics for $L=20$. This indicates that the instability of a stationary filament occurs via a subcritical Hopf bifurcation, and there is bistability between a stationary filament and periodic oscillations of a filament. For smaller L (e.g., $L=18$) this bifurcation becomes supercritical and the regime of bistability disappears. With increasing L the regime of complex spatiotemporal dynamics in the parameter space shrinks but the relative fraction corresponding to bistability expands. Complex dynamics does not occur for $L\gtrsim 270$.

Note that the phase diagrams in Fig. 6 depict only the asymptotic dynamics which can be reached using the uniform state as an initial condition. For some parameters the system exhibits bistability between different asymptotic regimes. Using a stationary filament as initial condition, one can detect bistability between stationary filaments and periodic oscillations of current filaments, as mentioned above, and bistability between periodic oscillations of current filaments and stable uniform limit cycles. The latter occurs only in a small regime of parameters near the intersection of curve 4 (temporal instability of current filament) and curve 3 (spatial instability of uniform limit-cycle oscillations). Generally, domains of bistability are found to be small compared to the whole regime of complex spatiotemporal dynamics. In the following subsections we describe periodic and chaotic modes of complex spatiotemporal dynamics which can be observed on square domains $L_x=L_y$.

B. Periodic spatiotemporal dynamics

Periodic spatiotemporal modes may occur as *breathing* or *spiking* current filaments [Figs. 7(a) and 7(b), respectively]. It is illustrative to visualize the different types of spatiotemporal dynamics in terms of their orbits in the projected phase space $(\langle J\rangle,u)$, in addition to invoking spatiotemporal plots and time series.

Periodic breathing represents a limit-cycle oscillation of the current filament amplitude [Fig. 7(a)]. In the parameter space periodic breathing follows upon stationary filaments with decreasing α and/or J_0. The Hopf bifurcation of a stationary filament leading to the onset of breathing can be either supercritical or subcritical. In the case of a supercritical bifurcation the amplitude of the breathing mode A increase as $A\sim\sqrt{J_0^{cr}-J_0}$. In the case of a subcritical bifurcation the onset of breathing occurs with finite amplitude and the stationary filament remains stable: in this case a stable breathing limit cycle appears simultaneously with an unstable breathing limit cycle which bounds the basin of attraction of the stable stationary filament.

Periodic spiking denotes the periodic formation and subsequent disappearance of a current filament [Fig. 7(b)]. Typically, between two spikes uniform small-amplitude damped oscillations occur. In the parameter space spiking appears with increasing J_0 following the uniform state [Fig. 6(a)]. Spiking is found when the uniform fixed point is spatially unstable $[L>L_{cr}(J_0)]$ but experiences no oscillatory instability. The stationary filament can be either unstable or stable for the parameters corresponding to spiking. In the first case the spiking mode is the only attractor, in the latter case there is bistability between two asymptotic states with different basins of attraction, but quasi-uniform initial conditions always lead to spiking.

Since the breathing mode results from a Hopf bifurcation of the stationary filament, it does not essentially interact with uniform modes related to damped or self-sustained oscillations. In contrast, spiking emerges from a spatial instability of the uniform steady state and its spatiotemporal dynamics may include slow linear stages when the current density distribution is nearly uniform. During those stages the system is sensitive to noise, and in large systems the period between spikes is likely to be determined by noise rather than by the internal dynamics. By changing the parameters, one can continuously transform breathing and spiking into each other, as for instance in the left upper corner of the phase diagram in Fig. 6(a), or induce chaotic dynamics. Chaotic scenarios will be discussed in the next subsection. Breathing is the only type of spatiotemporal dynamics which is observed for L close to $L_{\min}$, whereas spiking prevails with increasing L.

Breathing has been previously reported to occur in other models for current filamentation in semiconductors [46,47], with modifications which include drift terms with first order spatial derivatives in Eq. (1). Within the universality class covered by model (1),(4) it has been observed before only in 1D simulations with a concentration-dependent diffusion coefficient [48]. Spiking has been originally obtained in [38,42] on 1D domains. It has also been found experimentally [49].

C. Chaotic spatiotemporal dynamics: Period doubling, Shil'nikov chaos, and intermittency

Both breathing and spiking may become chaotic via period doubling [Figs. 8(a) and 8(b), respectively]. Breathing

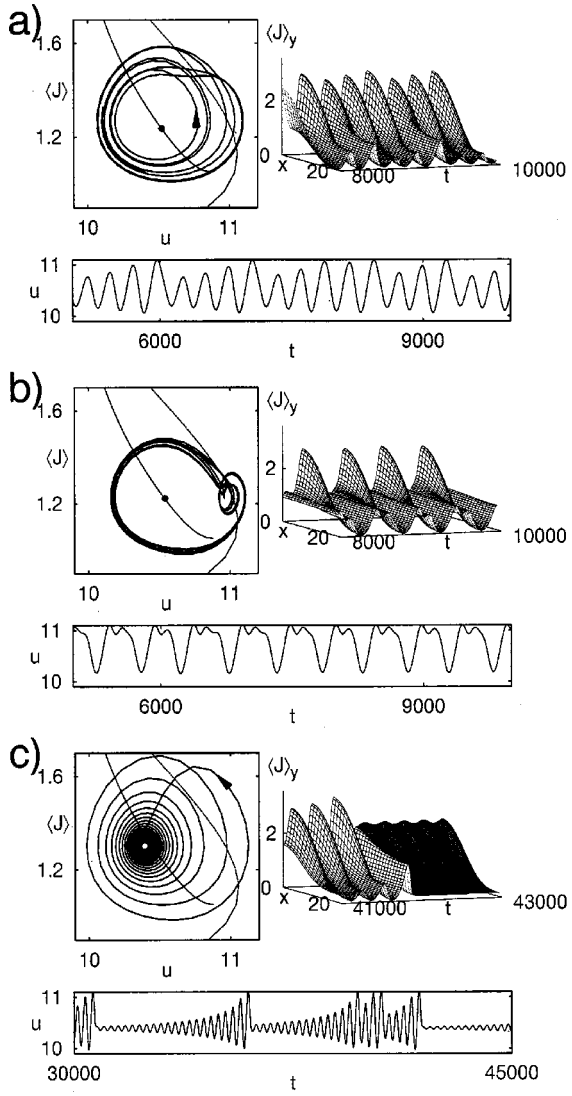

FIG. 8. (a) Chaotic breathing, (b) chaotic spiking of a corner filament on a 2D square domain ($L_x=L_y=20$, $\alpha=0.04$). Parameters (a) $J_0=1.27$, (b) $J_0=1.23$. (c) Special case of chaotic breathing due to a homoclinic orbit (Shil'nikov chaos). The saddle-focus corresponds to a weakly unstable stationary filament. Parameters: $J_0=1.302$, $\alpha=0.0368$, $L_x=L_y=20$. Same plots as in Fig. 7.

exhibits period doubling with decreasing α if J_0 is sufficiently large, and spiking does so with increasing J_0 if α is sufficiently small (see phase diagram in Fig. 6).

In the parameter regime corresponding to chaotic breathing there is a window where Shil'nikov chaos [50] is found (Fig. 8). In this window the stationary filament corresponds to a homoclinic saddle focus. The spatiotemporal dynamics in the vicinity of this fixed point can be understood in terms of linear eigenmodes of the stationary filament $\Psi_1(x,y)$ and $\Psi_2(x,y)$. The oscillatory instability is associated with an unstable ($\lambda_1>0$) ground-state eigenmode Ψ_1, corresponding to the voltage-controlled regime $u=$const. In the globally coupled regime, this mode is not suppressed by the global constraint for sufficiently slow inhibition ($\alpha<\lambda_1$), and two complex conjugate eigenvalues $\gamma\pm i\omega$ with $\gamma>0$ arise. The stable manifold of the saddle-focus is associated with the stable ($\lambda_2<0$) eigenmode Ψ_2 which dominates the formation of a current filament. Near the bifurcation point $\alpha\approx\alpha_f$ the spiralling-out of the trajectory from the homoclinic saddle-focus along the unstable manifold is slow compared to the return along the stable manifold, and therefore the Shil'nikov condition [50] $\gamma<|\lambda_2|$ holds, which ensures the existence of a chaotic attractor in the vicinity of the homoclinic orbit. The full dynamics includes two different stages, corresponding to motion along the stable and unstable manifolds of the saddle focus, respectively. The first, slow stage corresponds to breathing with slowly increasing amplitude; eventually the amplitude of breathing reaches the uniform fixed point in the projected phase space $(\langle J\rangle,u)$, and the current density distribution becomes almost uniform. During the next stage a rapid increase of transverse spatial perturbations returns the system to the unstable filamentary state. Such behavior can be observed in the tiny parameter regime near the point where the conditions for temporal filament instability and transverse spatial instability of a limit cycle coincide.

At the lower boundary of the regime of complex behavior [Fig. 6(a)] chaotic dynamics emerges via *intermittency* [Figs. 9(a),9(b)] due to the spatial instability of the uniform limit-cycle. Near the bifurcation line the respective intermittent regime resembles chaotic spiking [Fig. 9(a), see also Fig. 8(b)]. A similar intermittent regime has been found and analyzed in 1D simulations [42]. More sophisticated dynamics

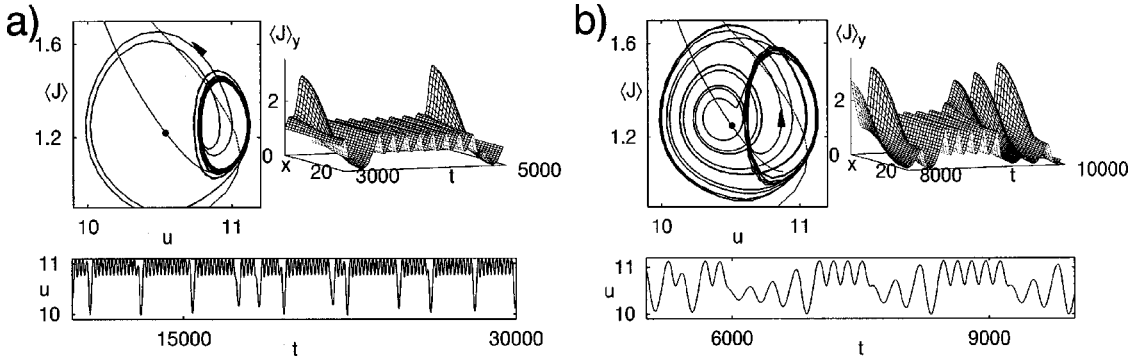

FIG. 9. (a) Intermittent spiking of a corner filament on a 2D square domain induced by a spatial instability of a uniform limit cycle. Parameters: $J_0=1.25$, $\alpha=0.032$, $L_x=L_y=20$. (b) Low-dimensional chaos induced by a temporal saddle-type instability of a corner filament combined with a spatial saddle-type instability of a uniform limit cycle. Parameters $J_0=1.28$, $\alpha=0.035$, $L_x=L_y=20$. Same plots as in Fig. 7.

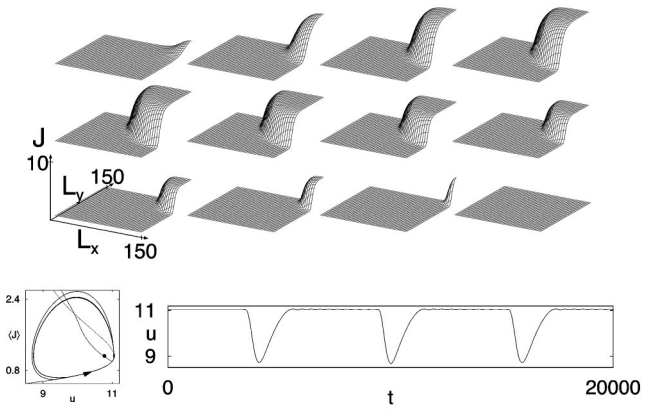

FIG. 10. Periodic back-and-forth motion of a current density front on a 2D square domain. Parameters $L_x=L_y=150$, $\alpha=0.005$, $J_0=1.13$. In the simulation spatially random persistent noise (amplitude $\delta a=0.0001$, interval between perturbations $\delta t=1000$) is added to trigger the instability of the uniform state. The 3D snapshots of the current density profile $J(x,y)$ are shown for times $t=15\,300$, $15\,360$, $15\,430$, $15\,500$, $15\,600$, $15\,700$, $15\,800$, $15\,900$, $16\,000$, $16\,100$, $16\,300$ (from upper left to lower right). The phase portrait $(\langle J\rangle,u)$, and the time series $u(t)$ is also depicted.

sets on if an oscillatory instability of the stationary filament also comes into play [Fig. 9(b)]. In this case the system has two saddle orbits with slow motion along their respective unstable manifolds: a spatially unstable uniform limit cycle and a temporally unstable filament. Quasiuniform periodic oscillations and a breathing current filament with increasing amplitude alternate at random. The example shown in Fig. 9(b) combines features of both Shil'nikov chaos [Fig. 8(b)] and intermittency [Fig. 9(a)]. Whereas in the vicinity of the uniform limit cycle the dynamics looks as in the intermittency regime, in the vicinity of the saddle focus corresponding to the stationary filament we observe the relatively slow oscillatory escape and fast return of the trajectory typical of Shil'nikov chaos [Fig. 8(b)]. The parameters corresponding to Fig. 9(b) have been specifically choosen to visualize the structure of the chaotic attractor in the most transparent way: the system has a heteroclinic orbit connecting the saddle focus with the saddle limit cycle. Nevertheless, in the general case the presence of two saddle orbits provides the basis for a variety of chaotic scenarios which dominate in the parameter regime corresponding to chaos for $L=20$.

D. Limit-cycle oscillations of a current density front

The regime of parameters corresponding to complex spatiotemporal dynamics shrinks as L increases (see Fig. 5), and the periodic spiking mode is the only one to survive in large systems. The spiking mode then starts to include expanding and shrinking of the filament as an intermediate stage between its nucleation and disappearance. For large systems ($L\gg L_{\min}$) the dynamics takes a well-pronounced form of back-and-forth motion of current density fronts (Fig. 10). This limit-cycle consists of four stages: first, the uniform intermediate state (a_0,u_0) looses stability with respect to transverse spatial perturbations and a small nucleus of the on-state (with characteristic size $L_{\min}$) embedded in the off-state is formed. In the second stage, the on-state expands via the propagation of a current density front. The expansion of the on-state continues approximately as long as u is larger than a critical value u_c which is correlated with the radius of the stationary corner filament (see Refs. [46,20] for a similar case in a drift-diffusion model). In the third stage, the voltage u drops below u_c and the direction of front propagation is reversed: now the on-state shrinks and finally disappears. For planar fronts an analogous scenario exists, and u_c corresponds to the voltage u_{co} where the on- and off-states coexist with a planar boundary; it is defined by the equal areas rule [33,35]

$$\int_{a_{\rm off}}^{a_{\rm on}} f(a,u_{co})\,da=0. \tag{19}$$

Here $a_{\rm on}$, $a_{\rm off}$ are the values of the variable a for on- and off-states, respectively. In the last stage, the dynamics is quasi-uniform and the system returns from the off-state to its initial unstable state (a_0,u_0). The relaxation of the current density distribution to the quasiuniform state is faster than the relaxation of the voltage u, hence during the last stage of the limit cycle the phase trajectory closely follows the off branch of the current-voltage characteristic. The nonuniform component of the current density distribution decreases and becomes very small when the system eventually reaches the unstable uniform state (a_0,u_0). As a result, the subsequent onset of the transverse instability is slow and the interval between consecutive spikes is large in comparison with the duration of a single spike. This implies that the period is actually determined not by internal dynamics but by persistent noise which should be taken into account in a realistic model.

Previously [30,32,33] we suggested that in bistable systems with one global constraint a purely temporal oscillatory instability of a current density front generally does not lead to limit-cycle motion of the front but eventually evolves into uniform oscillations. In contrast, our present findings reveal that limit-cycle front oscillations are possible near codimension-two points both on 2D and 1D domains.

IV. COMPLEX SPATIOTEMPORAL DYNAMICS ON RECTANGULAR DOMAINS

On rectangular domains ($L_x>L_y$) mixed spatiotemporal modes can be associated with both corner filaments [Fig. 3(a)] and edge current layers [Fig. 3(b)] parallel to the y axis. For $L_y<L_{\min}$ the current density is always uniform along the y axis rendering the dynamics effectively one-dimensional.

Let us now consider dynamics on 1D domains in more detail. We recall that filaments on a 1D domain of length L_x can be identified with edge current layers on a corresponding 2D domain with $L_x\gg L_y$. Complex spatiotemporal dynamics on 1D domains is found in a much larger parameter regime than on 2D domains with the same L_x [see Fig. 6(b)]. This is entirely due to the shift of the upper boundary (curve 4), which is associated with the temporal instability of the stationary filament. This shift means that corner filaments on 2D domains are more stable with respect to oscillations than 1D edge current layers for the same value of J_0: $\alpha_f^c>\alpha_f^e$, as can be seen in Fig. 4(b) in the relevant range of J_0. This also follows from the current-voltage characteristics shown in Fig. 3 since the eigenvalues are connected to the differential

conductance σ_d via Eq. (15). As a result, the sufficient condition for complex behavior $\alpha_f > \alpha_u$ can be met for 1D but violated for the corresponding 2D domain. We emphasize that the major difference in global dynamics on 1D and 2D domains is caused by quantitative changes in the linear dynamics near the stationary spatial structure, rather than near the uniform state (a_0, u_0).

Any 1D mode of complex spatiotemporal dynamics which occurs for a given $L_y < L_{\min}$ also exists for any $L_y > L_{\min}$. Those 1D modes have been found transversally unstable for $L_x \leqslant L_y$. However, they may become stable for $L_x > L_y > L_{\min}$. A typical phase diagram for a rectangular domain is shown in Fig. 6(c). The regime of complex spatiotemporal behavior is a subset of the respective regime for the 1D system with the same L_x [Fig. 6(b)]. Both 1D and 2D modes are possible. 1D oscillations of edge current layers occur for low values of α [Fig. 6(c)]. With increasing α we observe chaotic and periodic breathing of corner filaments, and the upper boundary of this regime matches the boundary of stability of the corner filament rather than that of the edge current layer. The transition from 2D complex oscillations of corner filaments to 1D complex oscillations of edge layers starts when the deviation from the square shape is small $[(L_x - L_y) \ll L_x, L_y]$ and is associated with an abrupt change of the type of spatiotemporal behavior, e.g., chaotic oscillation may be substituted by periodic ones, and vice versa. This might indicate that spatiotemporal behavior on 2D domains is generally not robust with respect to small variations of the domain shape.

V. CONCLUSIONS AND DISCUSSION

We have demonstrated that the competition between spatial and temporal instabilities may give rise to complex spatiotemporal dynamics of current density patterns in a globally coupled bistable semiconductor system on 2D spatial domains. Complex dynamics occurs near the codimension-two point in the parameter space where the uniform steady state simultaneously experiences a spatial instability leading to the formation of a stationary filament, and a Hopf bifurcation leading to onset of uniform limit-cycle oscillations. This point is analogous to the codimension-two Turing-Hopf point in the activator-inhibitor model (1), (2) with purely local coupling. Semiconductor systems generally exhibit subcritical bifurcations and formation of large-amplitude patterns [43,39,51,31] which are in many respects different from small-amplitude patterns that appear in chemical reaction models with polynomial nonlinearities [1,2,13,15]. Techniques based on an expansion in the vicinity of the uniform reference state can describe supercritical bifurcations, but fail to provide an adequate description of such subcritical patterns. Our approach is based on a linearization of the dynamics near both uniform and nonuniform (filamentary) states. This leads to a sufficient condition (17) for complex dynamics near the codimension-two point: the onset of mixed spatiotemporal modes is possible if the stationary filament exhibits an oscillatory instability for the parameters corresponding to the codimension-two bifurcation of the uniform state. For the opposite case $\alpha_f < \alpha_u$ we observe bistability between stationary patterns and uniform oscillations. Our model has two codimension-two points near the turning points of the S-shaped current-voltage characteristic [see Fig. 1(c)], but the condition (17) is met only near the one with the lower value of J_0.

The nonlinear dynamics has been studied numerically on square and rectangular 2D domains, including as a limit case 1D domains. In all cases complex spatiotemporal dynamics combines only two modes: the nonuniform mode related to a stationary current filament, i.e., a corner filament or an edge current layer, and a uniform mode related to damped or limit-cycle uniform oscillations. We have found three major types of periodic and chaotic spatiotemporal behavior: (i) periodic *breathing* of a current filament which appears as a result of a subcritical or supercritical oscillatory instability of a stationary filament and may evolve into a chaotic mode via period doubling; (ii) *spiking* of a current filament which results from the spatial instability of either the uniform steady state or uniform limit cycle oscillations. A special case of chaotic breathing appears when the system has a homoclinic orbit which is connected to a saddle focus corresponding to a weakly unstable stationary filament (Shil'nikov attractor). Another type of chaotic oscillations appears when two saddle-orbits—temporally unstable filament and spatially unstable uniform limit cycle—interact. (iii) We have also found periodic limit-cycle oscillations of current-density fronts resulting from a spatial instability of the uniform steady state in large systems.

We have shown that spatiotemporal spiking, which has previously been found only in 1D simulations of the model (6),(7) [38,42,49], is part of a much wider class of complex spatiotemporal modes which have been reported here for the first time. On square domains $(L_x = L_y)$ the only nonuniform mode is the one related to corner filaments, on rectangular domains $(L_x > L_y)$ oscillations of both corner filament and edge current layer parallel to the y axis are possible.

For fixed domain dimensions L_x, L_y the type of dynamics is determined by the parameters J_0 and α, which control the global level of excitation in the system and the relaxation time of the inhibitor u, respectively. In 1D systems complex spatiotemporal behavior can be observed in a much larger range of parameters compared to 2D systems. This is associated with a shift of the upper boundary of the regime corresponding to an oscillatory instability of the stationary filament, see Eq. (14): corner filaments on 2D domains are more stable with respect to oscillations than edge current layers in 1D systems. Therefore the transition from 1D domains to 2D domains is accompanied by a transition from the complex mixed mode regime (in 1D) to the regime of bistability between stationary patterns and uniform limit-cycle oscillation (in 2D) for a wide range of parameters. This qualitative difference results from quantitative changes in the linear dynamics near the stationary spatial pattern: the increment λ_1 of the first unstable mode decreases in going from 1D to 2D, thereby violating the criterion (17) on 2D domains.

The described scenarios of complex spatiotemporal behavior of current filaments are applicable to bistable systems whose internal state can be characterized by a *single* activator variable a and whose global inhibition is due to an external constraint. Another important mechanism for complex behavior occurs in systems with two mechanisms of inhibition acting on different time and space scales. The corresponding models are globally coupled two-component

activator-inhibitor systems [28,52,53], which are described by two internal local variables (activator and inhibitor) and one inhibiting global constraint and have local and global mechanisms of inhibition; and three-component activator-inhibitor models [51,54] with three local variables and two local mechanisms of inhibition. Depending on the hierarchy of relaxation times and diffusion lengths, complex behavior in the form of traveling [28,54], breathing [52], or spiking filaments [51] is found. These mechanisms of complex behavior are not related to degenerate bifurcations and can be expected to be more robust, but they are generally based on much more specific models and are therefore less universal. The analysis of experimental data shows that degenerate bifurcations [49] as well as multiple inhibition [51] can play a crucial role in complex dynamics, depending on the charge transport mechanism in a particular semiconductor system.

ACKNOWLEDGMENTS

We are grateful to W. Just and A. Wacker for valuable discussions. This work was supported by Deutsche Forschungsgemeinschaft in the framework of Sfb 555 and by Swedish Institute, Grant No. VISBY-380.

[1] J. P. Keener, Stud. Appl. Math. **55**, 187 (1976).
[2] H. Kidachi, Prog. Theor. Phys. **63**, 1152 (1980).
[3] I. Rehberg and G. Ahlers, Phys. Rev. Lett. **55**, 500 (1985).
[4] B. Zielinska, D. Mukamel, and V. Steinberg, Phys. Rev. A **33**, 1454 (1986).
[5] W. Zimmermann, D. Armbruster, L. Kramer, and W. Kuang, Europhys. Lett. **6**, 505 (1988).
[6] Q. Ouyang and H. L. Swinney, Chaos **1**, 411 (1991).
[7] J.-J. Perraud, K. Agladze, E. Dulos, and P. De Kepper, Physica A **188**, 1 (1992).
[8] P. De Kepper, J.-J. Perraud, B. Rudovics, and E. Dulos, Int. J. Bifurcation Chaos Appl. Sci. Eng. **4**, 1215 (1994).
[9] G. Heidemann, M. Bode, and H. Purwins, Phys. Lett. A **177**, 225 (1993).
[10] P. Kolodner, Phys. Rev. E **48**, R665 (1993).
[11] D. P. Valette, W. S. Edwards, and J. P. Gollub, Phys. Rev. E **49**, R4783 (1994).
[12] J.-J. Perraud, A. De Wit, E. Dulos, P. De Kepper, G. Dewel, and P. Borckmans, Phys. Rev. Lett. **71**, 1271 (1993).
[13] D. Lima, A. De Wit, G. Dewel, and P. Borckmans, Phys. Rev. E **33**, 1305 (1996).
[14] G. Dewel, P. Borckmans, A. De Wit, B. Rudovics, J.-J. Perraud, E. Dulos, J. Boissonade, and P. D. Kepper, Physica A **213**, 181 (1995).
[15] A. De Wit, D. Lima, G. Dewel, and P. Borckmans, Phys. Rev. E **54**, 261 (1996).
[16] M. Meixner, A. De Wit, S. Bose, and E. Schöll, Phys. Rev. E **55**, 6690 (1997).
[17] A. M. Turing, Philos. Trans. R. Soc. London **237**, 37 (1952).
[18] F. J. Elmer, Phys. Rev. A **41**, 4174 (1990).
[19] F. J. Elmer, Z. Phys. B: Condens. Matter **87**, 377 (1992).
[20] L. Schimansky-Geier, C. Zülicke, and E. Schöll, Z. Phys. B: Condens. Matter **84**, 433 (1991).
[21] L. Schimansky-Geier, C. Zülicke, and E. Schöll, Physica A **188**, 436 (1992).
[22] F. Mertens, R. Imbihl, and A. Mikhailov, J. Chem. Phys. **101**, 9903 (1994).
[23] M. Falcke, H. Engel, and M. Neufeld, Phys. Rev. E **52**, 763 (1995).
[24] D. Battogtokh and A. Mikhailov, Physica D **90**, 84 (1996).
[25] I. Schebesch and H. Engel, in *Self-Organization in Activator-Inhibitor Systems: Semiconductors, Gas Discharge, and Chemical Active Media*, edited by H. Engel, F.-J. Niedernostheide, H.-G. Purwins, and E. Schöll (Wissenschaft & Technik, Berlin, 1996), p. 120.
[26] M. Falcke and M. Neufeld, Phys. Rev. E **56**, 635 (1997).
[27] N. Mazouz, G. Flätgen, and K. Krischer, Phys. Rev. E **55**, 2260 (1997).
[28] F.-J. Niedernostheide, M. Or-Guil, M. Kleinkes, and H.-G. Purwins, Phys. Rev. E **55**, 4107 (1997).
[29] A. Alekseev, S. Bose, P. Rodin, and E. Schöll, Phys. Rev. E **57**, 2640 (1998).
[30] M. Meixner, P. Rodin, and E. Schöll, Phys. Rev. E **58**, 2796 (1998).
[31] A. V. Gorbatyuk and P. B. Rodin, Z. Phys. B: Condens. Matter **104**, 45 (1997).
[32] M. Meixner, P. Rodin, and E. Schöll, Phys. Rev. E **58**, 5586 (1998).
[33] M. Meixner, P. Rodin, E. Schöll, and A. Wacker, Eur. Phys. J. B **13**, 157 (2000).
[34] A. F. Volkov and S. M. Kogan, Sov. Phys. Usp. **11**, 881 (1969).
[35] E. Schöll, *Nonequilibrium Phase Transitions in Semiconductors* (Springer, Berlin, 1987).
[36] B. Glavin, V. Kochelap, and V. Mitin, Phys. Rev. B **56**, 13 346 (1997).
[37] D. Mel'nikov and A. Podivaev, Semiconductors **32**, 206 (1998).
[38] A. Wacker and E. Schöll, Z. Phys. B: Condens. Matter **93**, 431 (1994).
[39] A. V. Gorbatyuk and P. B. Rodin, Solid-State Electron. **35**, 1359 (1992).
[40] E. Schöll, *Nonlinear Spatiotemporal Dynamics and Chaos in Semiconductors* (Cambridge University Press, Cambridge, in press).
[41] A. Wacker and E. Schöll, J. Appl. Phys. **78**, 7352 (1995).
[42] S. Bose, A. Wacker, and E. Schöll, Phys. Lett. A **195**, 144 (1994).
[43] B. S. Kerner and V. V. Osipov, *Autosolitons* (Kluwer Academic Publishers, Dordrecht, 1994).
[44] F. G. Bass, V. S. Bochkov, and Y. G. Gurevich, Zh. Éksp. Teor. Fiz. **58**, 1814 (1970) [Sov. Phys. JETP **31**, 972 (1970)].
[45] E. Schöll, Z. Phys. B: Condens. Matter **62**, 245 (1986).
[46] E. Schöll and D. Drasdo, Z. Phys. B: Condens. Matter **81**, 183 (1990).
[47] R. E. Kunz and E. Schöll, Z. Phys. B: Condens. Matter **89**, 289 (1992).
[48] A. Wacker and E. Schöll, Supercond. Sci. Technol. **9**, 592 (1994).
[49] F.-J. Niedernostheide, H. Schulze, S. Bose, A. Wacker, and E.

Schöll, Phys. Rev. E **54**, 1253 (1996).
[50] J. Guckenheimer and P. Holmes, *Nonlinear Oscillations, Dynamical Systems, and Bifurcations of Vector Fields*, Vol. 42 of *Applied Mathematical Sciences* (Springer-Verlag, Berlin, 1983).
[51] B. Datsko, Semiconductors **31**, 146 (1997).
[52] F.-J. Niedernostheide, M. Ardes, M. Or-Guil, and H.-G. Purwins, Phys. Rev. B **49**, 7370 (1994).
[53] F.-J. Niedernostheide, C. Brillert, B. Kukuk, H.-G. Purwins, and H.-J. Schulze, Phys. Rev. B **54**, 14 012 (1996).
[54] C. P. Schenk, M. Or-Guil, M. Bode, and H.-G. Purwins, Phys. Rev. Lett. **78**, 3781 (1997).